A&A manuscript no.
(will be inserted by hand later)

Your thesaurus codes are:
02.01.4; 02.12.1; 03.20.8; 09.09.1 SNR 1E 0102.72.3 ; 11.13.1; 13.25.4

ASTRONOMY AND ASTROPHYSICS

The X–Ray Spectrum of the Supernova Remnant 1E 0102-72.3

Andrew P. Rasmussen[1] Ehud Behar[1] Steven M. Kahn[1] Jan Willem den Herder[2] and Kurt van der Heyden[2]

[1] Columbia Astrophysics Laboratory 550 West 120th Street, New York, NY 10027 U.S.A.
[2] University of Utrecht and Space Research Organization of the Netherlands Sorbonnelaan 2, 3584 CA Utrecht, NL

Received September 15, 2000; accepted March 16, 1997

Abstract. In this letter we present the soft X–ray (5-35Å) spectrum of the supernova remnant (SNR) 1E 0102-72.3 in the Small Magellanic Cloud, acquired by the reflection grating spectrometer (RGS) aboard ESA's *XMM-Newton Observatory*. This extended–source X–ray spectrum of unprecedented spectral resolution ($\lambda/\Delta\lambda \sim 300$) permits, for the first time, unambiguous identification and measurement of isolated emission lines and line complexes alike. The diagnostic power of performing spectroscopy using groups of emission lines from single ions is exemplified. In particular, the bright Lyman and helium series lines for light elements (C VI, O VII, O VIII, Ne IX, Ne X and possibly Mg XI & Mg XII) show peculiar ratios, where the values [1s − np] / [1s − (n + 1)p] are systematically weaker than expected for electron impact excitation. These measured ratios resemble signatures of recombining or charge exchanging plasmas. We argue that charge exchange, given its large cross section and evidence for inhomogenious media within the SNR, is a likely mechanism for the observed emission. Also, the well known temperature diagnostics $G(T_e) = (i+f)/r$ of helium–like triplets (O VII & Ne IX) indicate high temperatures, well above the maximum emission temperature T_m for each ion, and consistent with a purely ionizing plasma. The density diagnostics $R(n_e) = f/i$ meanwhile, are consistent with the low density limit, as expected.

Key words: Atomic processes – Line: formation – ISM: individual objects: 1E 0102-72.3 – Galaxies: Magellanic Clouds – X-rays: ISM

1. Introduction

The supernova remnant 1E 0102-72.3 (E0102) is a bright, oxygen–rich remnant located in the Small Magellanic Cloud (SMC), approximately 60 kpc distant. Although it is young (~ 1000 years old) and clearly very energetic, it has no bright emission lines of Fe K nor significant continuum above 5 keV. It has received substantial attention recently, with the availability of high quality *Chandra* data (Gaetz et al., 2000; Hughes et al., 2000) as well as *Hubble Space Telescope* data (Blair et al., 2000). Its ionization structure in terms of spatial stratification was clearly seen for the first time with *Chandra* (Gaetz et al., 2000), and details of the outgoing blast wave's kinematics and emission spectrum were used to argue that a large fraction of E0102's energy is spent toward cosmic ray acceleration (Hughes et al., 2000). It was also observed with the *High Energy Transmission Grating Spectrometer* aboard *Chandra* to explore the spatially resolved, line of sight velocity structures to isolated emission lines in the spectrum, which help to elucidate the initial geometry and mass distribution of the initial supernova event, as well as probe the kinetics of various spectrally resolved components making up the SNR structure (Flanigan, 2000; Canizares, 2000).

In our work, we concentrate on the high resolution X–ray spectroscopy afforded by the RGS (den Herder et al., 2000) aboard *XMM-Newton* (Jansen et al., 2000), which performs with nearly nominal spectral resolution, even for extended objects such as E0102: We observe using the RGS to address the emission mechanism of the SNR.

2. Observation and Data Analysis

E0102 was observed early in *XMM-Newton's* Calibration phase, during revolution 0065 (16 April, 2000) for a total of 42.8 ksec. All three EPIC (Turner et al., 2000; Struder et al., 2000) instruments and both RGS (den Herder et al., 2000) instruments were operated simultaneously. Here, our primary focus is on the high resolution X–ray spectrum of E0102, and we restrict attention to the RGS data[1].

The data were processed using custom software, originally developed for the analysis of RGS ground calibration data, which is nearly identical in function to the RGS branch of the Science Analysis System (SAS). Telemetered CCD events were read in,

Send offprint requests to: A. Rasmussen
Correspondence to: arasmus@astro.columbia.edu

[1] A separate letter on the EPIC observation of E0102 is included in this volume (Sasaki et al., 2000).

frame by frame for each CCD node, and were offset corrected on a pixel by pixel basis using median readout maps, compiled from about 40 DIAGNOSTIC (den Herder et al., 2000) images per CCD chip. This process nearly eliminates flickering pixels from the dataset. Gain and CTI corrections were performed to align the signal/energy scale across all CCD readouts. Then, event reconstruction was performed on *connected* pixels containing significant signal, and the composite event signals were calculated by summing up signals from individual pixels.

The standard event grade combinations used were those which fall within a 2 × 2 pixel region, where two pixels diagonally opposed to one another within the 2 × 2 were not grouped into composites. The event coordinates were then mapped into focal plane angular coordinates (dispersion and cross–dispersion)[2]. Using the star tracker attitude history updates for the revolution, the coordinates of the source, and a prelminary boresight axis, aspect corrections were applied to the focalplane event angular coordinates.[3]

Events were extracted in the dispersion–pulseheight plane with masks utilized by the response matrix generator. The surviving events were then windowed in the focal plane, where background subtraction was performed using background sampling regions off to one side of the illumination pattern in the cross–dispersion direction.[4] The size of the spatial extraction was 58″ in the cross–dispersion direction, which comfortably includes the entire spectrum. A spectrum file was created by computing the background corrected countrates in each dispersion channel. Finally, a response generator was used to produce an observation specific response matrix that provided an array of nominal wavelength/energy values corresponding to each channel in the spectrum file. Line fluxes were estimated by comparing an emission model, folded through the response matrix, directly to the spectrum in the usual manner. This procedure was performed for first (m=-1) and second (m=-2) orders for each spectrometer.

To reduce the contamination from sporadic background rate fluctuations in which the RGS counting rate doubles from the quiescent rate of about 1 ct s^{-1} RGS^{-1}, a set of good time intervals (GTIs) were chosen to filter out the high background data. This reduced the effective exposure time from 37.9 to 29.7 ksec for both RGS instruments.

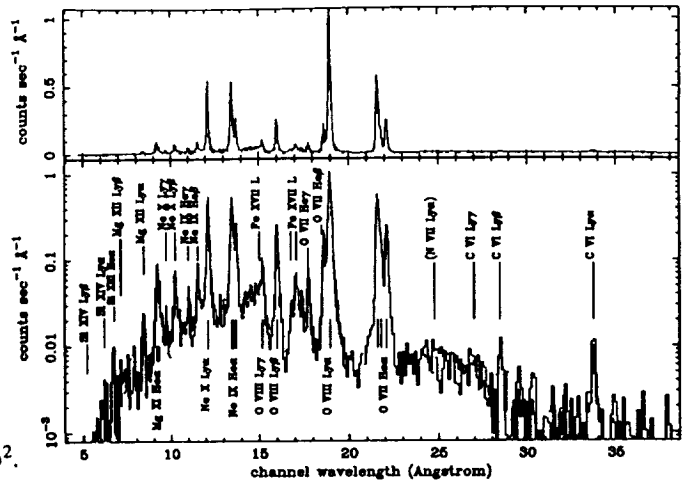

Fig. 1. The first order (m=–1) RGS spectrum of E0102. The data obtained from the two RGS instruments are plotted separately (RGS1 in black, RGS2 in red). The 20–24Å gap in the RGS2 spectrum is due to failed electronics for CCD 4 in that instrument. For clarity, the data are provided in both linear and logarithmic scales. Identifications of the principle lines are provided.

The windowed background contribution to the (m=-1) total countrate for this extraction was nearly flat, at 2.3×10^{-5} ct s^{-1} chan^{-1} or, equivalently, 2.3×10^{-3} ct s^{-1} Å^{-1} at 15Å[5].

3. The Soft X–Ray Spectrum of 1E 0102-72.3

Using the analysis procedure described above, we generated the RGS spectra shown in Figures 1 and 2. The spectrum is dominated by a small number of emission lines, the brightest of which are resonance transitions of highly stripped light ions. Nitrogen, which is cosmically less abundant than oxygen by a factor of a few, is is absent in our spectrum (N VII Lyα is expected at 24.7Å). Only very weak Fe L lines are detected, which are dwarved by the strong transitions of the light, even Z elements. We detect bright lines from the Lyman series of C VI, O VIII, Ne X and Mg XII, and from the helium series of O VII, Ne IX, Mg XI and Si XIII. Most of these ions are represented by several emission lines in the spectrum, clearly resolved and measurable in this phenomenally clean spectrum. Single ion spectroscopy permits independent measures of astrophysical quantities that affect line production, such as electron temperature and density, or radiative transport within the object and in any intervening material.

To synthesize the appropriate RGS response for E0102, we need to quantify the angular distribution of the X–ray emission, which is convolved with the other quantities contributing to the line spread function. As a preliminary approximation, we used a public *Chandra* image (ObsIds 1231 & 1423) as an energy independent distribution, characterized by ~20″ HEW and ~33″

[2] The dispersion coordinates are based on the known geometry of the RGS within *XMM-Newton* (den Herder et al., 2000).

[3] Based on attitude history updates of the star tracker system, the spacecraft pointing was extremely steady, drifting only 0.1″ and 0.2″ (rms) in the dispersion and cross–dispersion axes, respectively, over the observation. The respective peak–to–peak attitude swings were only 0.5″ and 0.7″.

[4] The target was ~ 1′ off–axis in cross–dispersion, so the spectrum illuminated the RGS focalplane camera on one side of the CCD array. Consequently, background sampling was performed in an asymmetric manner.

[5] Also equivalent to 1.4×10^{-4} ct s^{-1} per resolution element. This is higher than the typical background level because of the enlarged extraction volume for this target.

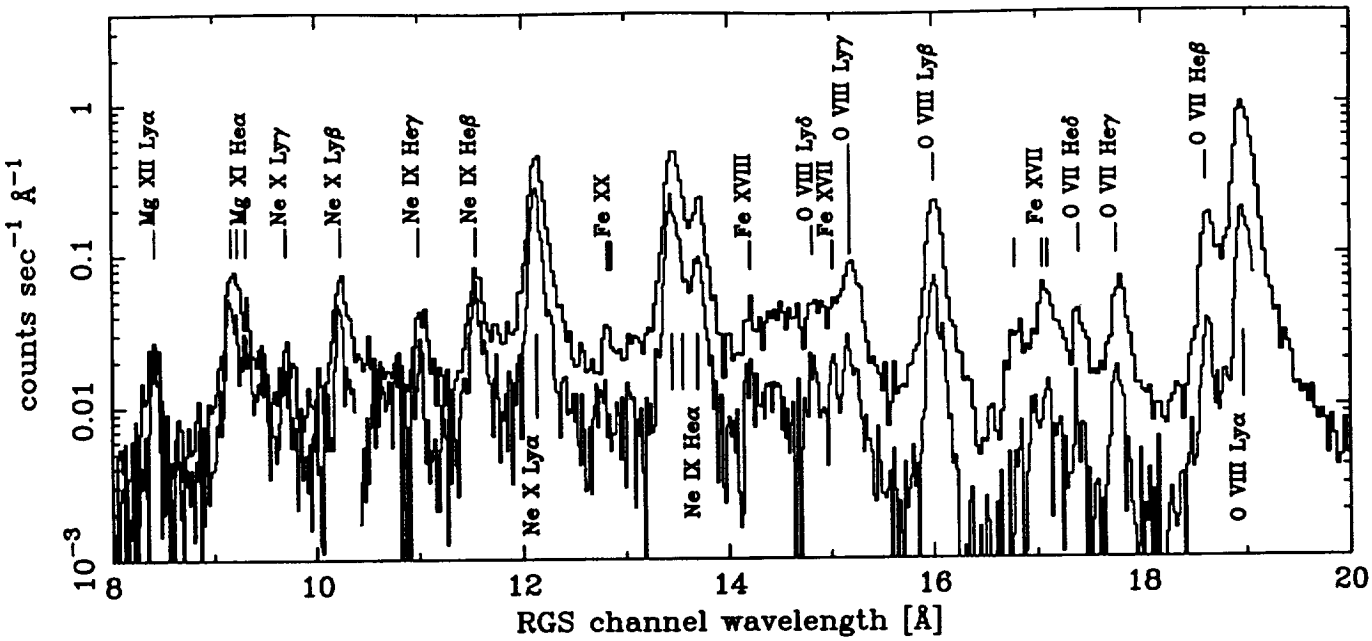

Fig. 2. Detail of the 8–20Å region of the RGS data. First and second order extractions are plotted separately (m=–1 in black, m=–2 in red) to facilitate line identification. The data from the two spectrometers have been averaged for each order extraction. The higher spectral resolution and resilience to source extent in is clearly seen in m=–2, where some line complexes blended in m=–1 are resolved.

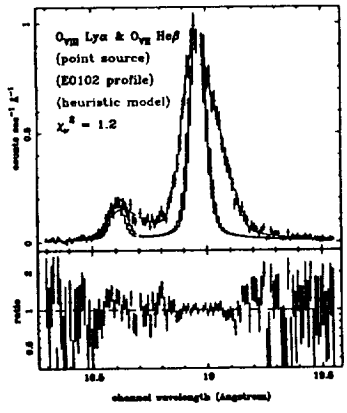

Fig. 3. Illustration of the line profile used for estimating line fluxes. The plot compares the point source line spread function for RGS1, the approximate monochromatic line profile based on E0102's angular distribution (derived from the *Chandra* image), and an heuristic wavelength broadening template function that is applied in addition to the angular distribution.

FWHM. The image was collapsed along the dispersion axis according to the roll of *XMM-Newton* during the observation. This 1–dimensional distribution was used as input to the response generator. Comparing the prediction to the brightest, isolated emission line (O VIII Lyα), we see that the prediction is far narrower than the data, indicating a velocity distribution resolved by the RGS (see Fig. 3). Further accurate modeling requires coupling a line of sight velocity distribution to the angular distribution, but for the time being we are able to place a lower limit to the ejecta's expansion, 1350 km s^{-1}, using the square velocity profile model of an expanding shell. This lower limit is consistent with the broadening seen in all of the lines. To proceed with spectral modeling, we use this distribution as a template for line modeling and flux estimation.

We attempt to remove the effects of intervening absorption from the line intensities. The self consistent absorption column used is derived by fitting the long wavelength part of the spectrum (see the slope of the continuum in Fig. 1) with an absorbed bremsstrahlung component hot enough to produce the Oxygen lines. The derived column ($N_H = 1.6 \times 10^{21}$ cm^{-2}) is twice the Galactic column toward the SMC and other estimates of absorption column toward E0102 (Blair et al., 1989; Hayashi et al., 1994; Blair et al., 2000). Absorption corrected line flux ratios are given in Figure 4 for multiple lines produced by the same ion. The line ratios inferred from the data are far from predictions for a collisionally excited, optically thin thermal plasma. As shown in the figure, the predicted intraseries

Table 1. Absorption corrected emission line ratios for single ion series, for 1E 0102-72.3. These ratios include resonant transitions only. The value used for N_H was 1.6×10^{21} cm^{-2}, using solar abundances. Naturally, these ratios depend on the value of N_H assumed, particularly for C VI and O VII. Figure 4 plots these ratios along with predicted ratios for CIE. Sample charge exchange (CE) measurements are included for O VIII Lyman line ratios (Bliman et al., 1985), provided here for the discussion below.

line ratio	*Carbon*	*Oxygen*	*Neon*
He α (*w*)/He β	NA	6.3 ± .25	7.9 ± .47
(CIE)		(9.2)	(8.9)
He β/He γ	NA	2.6 ± .23	2.2 ± .18
(CIE)		(3.2)	(3.1)
Ly α/Ly β	5.2 ± .52	6.8 ± .27	7.4 ± .37
(CIE)	(12.5)	(11.3)	(10.6)
(CE, $O^{+8} + H_2$)		(4.2)	
Ly β/Ly γ	NA	2.8 ± .17	2.9 ± .29
(CIE)		(4.4)	(4.1)
(CE, $O^{+8} + H_2$)		(3.1)	
Ly α/He α (*w*)	NA	1.35 ± .04	0.84 ± .03

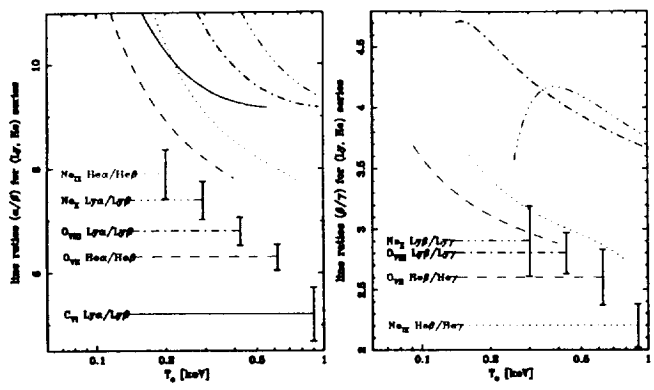

Fig. 4. Emitted line ratios. Plotted are the absorption corrected line ratios for adjacent emission lines for individual ions from Table 1, compared to line ratios expected from thermal plasma models. The left hand plot shows the ratios of Lyα/Lyβ (C VI, O VIII & Ne X) and Heα(r)/Heβ (O VII & Ne IX); the right hand plot gives Lyβ/Lyγ (O VIII & Ne X) and Heβ/Heγ (O VII & Ne IX). The measured ratios are plotted as horizontal lines with error bars and the curves show the temperature dependence to these line ratios, assuming a CIE model. If contributions from recombination were turned off (the case of a purely ionizing plasma or strong NEI, for example), the curves would move up in value, particularly at the high T_e end.

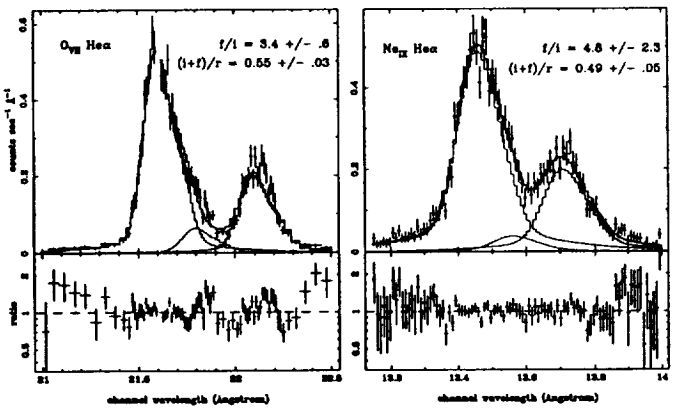

Fig. 5. Derivation of the R (density) and G (temperature) line ratio diagnostics for O VII (left) and Ne IX (right). The data were fit using three line features, where we have used the heuristic wavelength distribution function derived from O VIII Ly α as a template to describe each (see Fig. 3). One parameter adjusted the ensemble line position (relative line positions were fixed), and the three line intensities were allowed to vary to fit the data. Individual contributions from the f, i and r lines are shown. The χ^2_ν values are 1.4 and 0.9 for the O VII and Ne IX triplets, respectively.

ratios α/β and β/γ for heliumlike and hydrogenlike ions are dependent on T_e, but asymptotically approach their minimum values in the limit of high temperature. Our measured ratios are significantly below these high temperature limits, for every ion species. It is curious to note that the measured ratios are similar to the expected line ratios from a recombining plasma.

In spite of the angular extent of the source and the velocity broadening of the lines, we resolve the Heα line complexes of O VII, Ne IX and Mg XI sufficiently to estimate contributions from the forbidden, intercombination and resonance transitions that provide robust diagnostics for the temperature and density of the emitting medium (Gabriel and Jordan, 1969; Pradhan, 1982; Porquet and Dubau, 2000). Figure 5 shows the heliumlike triplets of O VII and Ne IX, modelled using the known line wavelengths, and the line velocity profile adopted above (Fig. 3). While the density diagnostic R ratios obtained were reasonable and consistent with the low density limit at the 90% confidence level, the temperature diagnostic G values are low. They are measured at $0.55 \pm .03$ and $0.49 \pm .05$ for O VII and Ne IX, respectively. The electron temperatures corresponding to these ratios are 0.35 and 0.65 keV for O VII and Ne IX respectively (Pradhan, 1982), significantly above the maximum line producing temperatures (T_m) for each ion. These high temperatures are far from equilibrium temperatures where these ions are abundant, and suggest a purely ionizing plasma where the plasma is underionized and recombination rates are suppressed by the high T_e.

4. Discussion

The Fe L lines that we do see in the SNR most likely trace the swept up ISM rather than the ejecta of the precursor. The Fe:O abundance ratio that we measure is about 1:900, compared to 1:15 or so in the SMC (Russell and Dopita, 1992). With the exception of the Fe, the composition of the SNR is dominated by products of He burning, the SN ejecta. The absence of emission from N is suggestive that any nitrogen in the progenitor had been either blown off or burned into other products.

The measured values for intraseries, single ion line flux ratios α/β and β/γ are unexpected. They are not consistent with any T_e capable of collisionally exciting the lines seen, nor any combination of such distributions. They are also far from values predicted from previous modeling efforts for adiabatic SNRs evolving through nonequilibrium ionization (Hamilton et al., 1983).

We have been unable to identify any likely mechanisms by which an emitted electron impact excitation spectrum could be modified by selective absorption to produce the line ratios measured. Invoking an additional absorber fails: an intervening neutral absorber, used to explain the observed flux ratio predicts columns different by $N_H \sim 10^{21}\,\mathrm{cm}^{-2}$ between O VII and O VIII, which is clearly implausible. The possibility of the embedded gas working as an absorber is easily rejected: if significant, sharp increases in the Lyα/Lyβ ratios for O VIII and Ne X, are expected due to the K edge energies of O VII and Ne IX, which are not seen.

The possibility is remote that resonant line scattering in the presence of a dusty or photoelectrically absorbing medium allows for the selective destruction of the large oscillator strength lines. In the approximation of total frequency redistribution, resonantly scattered photons are reemitted according to the doppler distribution of the gas, and the photon is likely to escape in τ_0 scatterings (where τ_0 is the optical depth at the line peak). The probability of being absorbed between scatters is τ_{abs}/τ_0, so

the fraction absorbed prior to escape is approximately τ_{abs}, independent of line oscillator strength. Even in the case of total coherence, where escape is likely after τ_0^2 scatters, the absorbed fraction is $\tau_{abs}\tau_0$ and we would expect the discrepancies in line ratios[6] to scale with the ratios of oscillator strengths, which is not seen.

As mentioned above, the line ratios, with the exception of the G ratios obtained for heliumlike ions, are reminiscent of a recombining plasma. Similar line ratios are also expected from charge exchange (Wise and Sarazin, 1989), where the exchanged electrons are injected into specific high (n, l) levels according to energy conservation and details of the transient valence bonds formed between exchange partners. Spectra from such reactions have been observed extensively in tokamak and ion beam experiments, for example, in highly ionized Ar^{+18} (Rice et al., 1986) and O^{+8} (Bliman et al., 1985). In the latter work, charge exchange reactions of O^{+8} with molecular H_2 yielded values of $Ly\alpha/Ly\beta \sim 4.2$ and $Ly\beta/Ly\gamma \sim 3.1$ (40% relative error in each) and a preferential injection into $n = 5$. Calculations performed for interactions with atomic hydrogen yield values with comparable variances, but all well below the ratios predicted by electron impact excitation.

In order for charge transfer to contribute significantly to the X–ray line emission from a SNR, low ionization species (neutral hydrogen or helium, or singly ionized helium) must come into close proximity with more heavily ionized metals (i.e., fully stripped carbon, oxygen, and neon, for this case). Given that the charge exchange and electron impact excitation rate coefficients are of order $\gamma_{CE} \sim 10^{-6}$ and $\gamma_{EIE} \sim 10^{-11}$ cm^3 s^{-1}, respectively, charge exchange can be important if the neutral fraction for hydrogen is greater than $\sim 10^{-5}$ or so (Wise and Sarazin, 1989). Unfortunately, this is well above the neutral fraction expected for the hot ionized plasma where the X–ray emission is thought to originate.

However, there is abundant evidence that the X–ray emitting media in SNRs are far from homogenious. Cool clouds can coexist in rough pressure balance with the hotter intercloud medium. One therefore expects a steady flux of highly ionized material from the hot medium at the "faces" of each of the clouds. These ions will charge exchange with neutral hydrogen in the clouds, giving rise to X–ray emission lines. Since the charge exchange cross–section for the ions is considerably larger than the photoelectric absorption cross-section for the emitted line photons, the emitted line radiation should emerge and contribute to the observed X–ray spectrum of the remnant. This process should be important if the mean intercloud separation is smaller than the characteristic distance d an ion will move through the hot gas before it is collisionally excited:

$$d = 1.0\,\mathrm{pc}\left(\gamma_{EIE}/10^{-11}\right)^{-1} T_{\mathrm{keV}}^{1/2} A_{\mathrm{AMU}}^{-1/2} n_e^{-1}. \quad (1)$$

The *Chandra* image of E0102 (Gaetz et al., 2000) exhibits significant structure on spatial scales comparable to or less than this value. It therefore seems likely that charge exchange at cloud interfaces plays a significant, if not dominant role in producing the anomalous line ratios that we observe.

Acknowledgements. Based on observations obtained with *XMM-Newton*, an ESA science mission with instruments and contributions directly funded by ESA Member States and the USA (NASA).

[6] The effect on α/β ratios should be about twice the effect on β/γ ratios.

References

Blair, W. P., Morse, J. A., Raymond, J. C., Kirshner, R. P., Hughes, J. P., Dopita, M. A., Sutherland, R. S., Long, K. S., and Winkler, P. F., 2000, ApJ 537, 667

Blair, W. P., Raymond, J. C., Danziger, J., and Matteucci, F., 1989, ApJ 338, 812

Bliman, S., Bonnet, J. J., Montenesquieu, A. B., Dousson, S., Druetta, M., Hitz, D., and Mayo, M., 1985, Nucl. Instrum. Methods Phys. Res., Sect. B 9, 371

Canizares, C., 2000, in R. Giacconi, L. Stella, and S. Serio (eds.), X-Ray Astronomy 2000, Publications of the Astronomical Society of the Pacific Conference Series, PASP

den Herder, J. W., several, other, and authors, 2000, A&A p. this volume

Flanigan, K., 2000, in R. Giacconi, L. Stella, and S. Serio (eds.), X-Ray Astronomy 2000, Publications of the Astronomical Society of the Pacific Conference Series, PASP

Gabriel, A. H. and Jordan, C., 1969, MNRAS 145, 241

Gaetz, T. J., Butt, Y. M., Edgar, R. J., Eriksen, K. A., Plucinsky, P. P., Schlegel, E. M., and Smith, R. K., 2000, ApJ 534, L47

Hamilton, A. J. S., Sarazin, C. L., and Chevalier, R. A., 1983, ApJS 51, 115

Hayashi, I., Koyama, K., Ozaki, M., Miyata, E., Tsunemi, H., Hughes, J. P., and Petre, R., 1994, PASJ 46, L121

Hughes, J. P., Rakowski, C. E., and Decourchelle, A., 2000, ApJ in press

Jansen, F., several, other, and authors, 2000, A&A p. this volume

Porquet, D. and Dubau, J., 2000, A&AS 143, 495

Pradhan, A. K., 1982, ApJ 263, 477

Rice, J. E., Marmar, E. S., Terry, J. L., Kallne, E., and Kallne, J., 1986, Phys. Rev. Lett. 56, 50

Russell, S. C. and Dopita, M. A., 1992, ApJ 384, 508

Sasaki, M., several, other, and authors, 2000, A&A p. this volume

Struder, L., several, other, and authors, 2000, A&A p. this volume

Turner, M., several, other, and authors, 2000, A&A p. this volume

Wise, M. W. and Sarazin, C. L., 1989, ApJ 345, 384